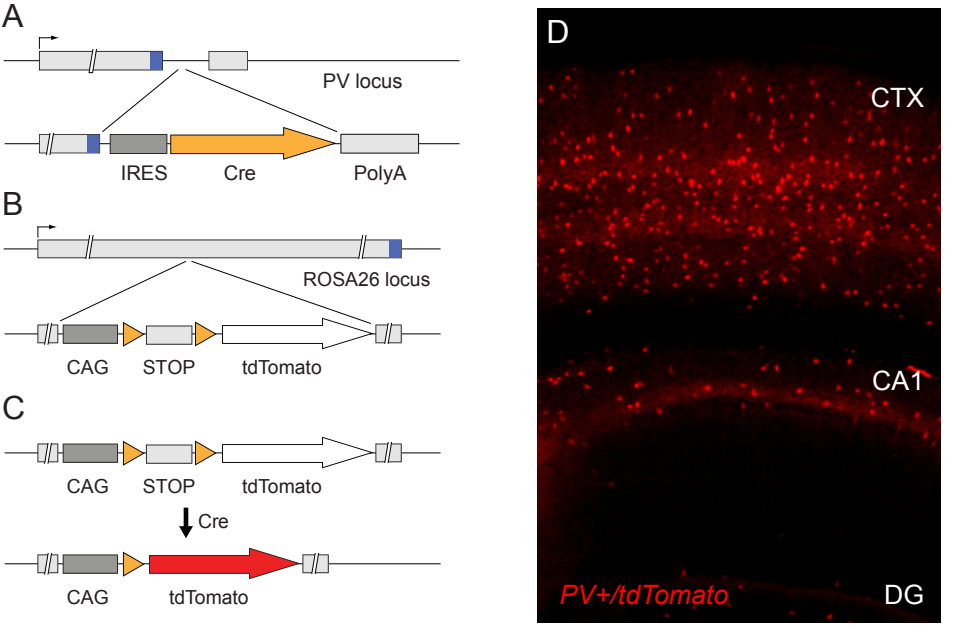


**Supplementary Figure 1: Schematic for generating *PV-Cre;Ai14* mice, see FIgure 1**

Knock-in *PV-Cre* animals (A, see Methods) are mated to knock-in tdTomato *Cre reporter* mice (Ai14; Madisen et al. 2010), in which a fluorescent protein expression cassette inserted into the ROSA26 locus is interrupted by a floxed transcription termination domain (STOP) (B). PV+ neurons in the progeny are selectively labeled with tdTomato (C) after the STOP sequence is excised. (D) Representative coronal section encompassing portions of cortical V1 (CTX), dorsal hippocampal CA1, and dentate gyrus (DG) from a *PV-Cre;Ai14* animal. PV+ neurons within each region express tdTomato.

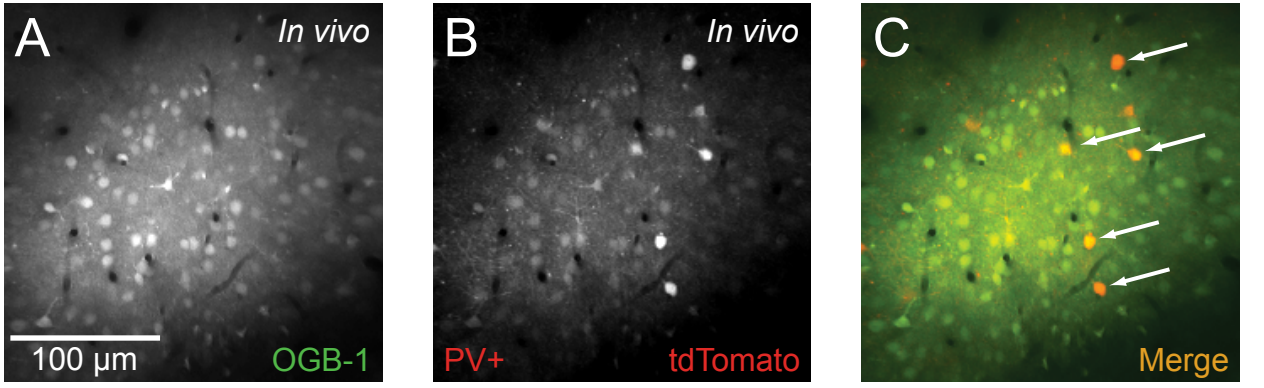


**Supplementary Figure 2: Additional example (see Figure 1) of two-photon imaging in vivo and identification of PV+ interneurons**

(A) Two-photon image of OGB-1 *in vivo*. (B) Same as in (a) for tdTomato. (C) Merge of OGB-1 and tdTomato. Cells with co-localized fluorescence (putative PV+ interneurons) appear yellow (*arrows*).

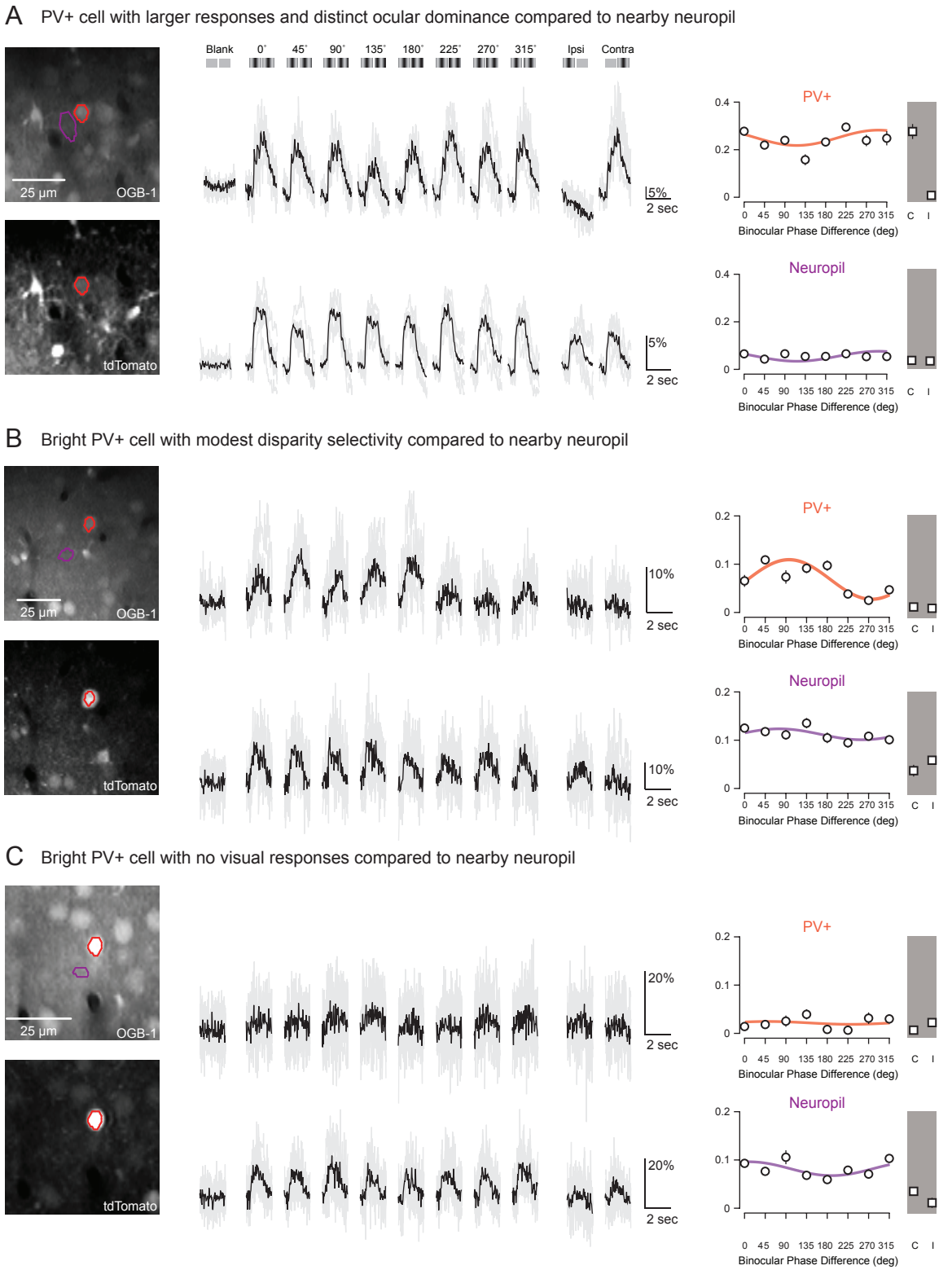


**Supplementary Figure 3: Additional examples of binocular and monocular responses in PV+ interneurons and local neuropil, see Figure 2**

(A) Example monocular PV+ cell with large responses and distinct ocular dominance compared to local neuropil activity. Identified cell (red) and neuropil ROI (purple) shown in OGB-1 and tdTomato structural images (*left*). Individual trial and mean responses (gray and black, respectively) for the PV+ cell and neuropil are shown (*middle*) for blank periods, binocular stimuli, and monocular stimuli. Peak responses and disparity tuning are also shown for PV+ cell and neuropil (*right*). (B) Same as in (A) for an example PV+ cell with strong tdTomato-expression exhibiting modest disparity sensitivity in binocular responses and no monocular responses. These neural responses are in contrast to nearby neuropil activity, which is binocular and untuned for disparity. (C) Same as in (A) for an unresponsive PV+ cell with strong tdTomato-expression. Nearby neuropil activity is visually responsive during each stimulus condition.

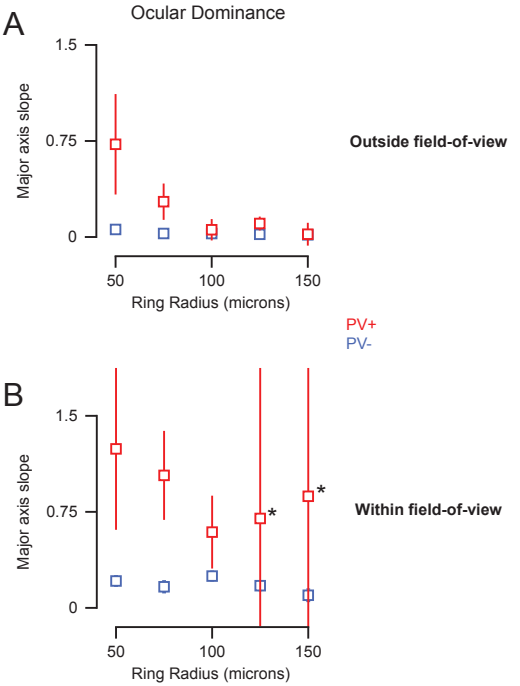


**Supplementary Figure 4: PV+ spatial relationship is maintained for local populations excluding or only including neighboring neurons within the same field-of-view (see Figure 4).**
(A) Spatial relationship between individual cell ocular dominance and local population average ocular dominance. In these data, local populations include only cells outside the field-of-view (z-plane) of individual cell. Shown is mean Bootstrapped PCA slopes and standard error for PV+ interneurons (red) and PV- neurons (blue). (B) Same as in (a), but with local population averages computed from only cells within the same field-of-view as individual cell. Asterisks indicate data with truncated standard error bars.

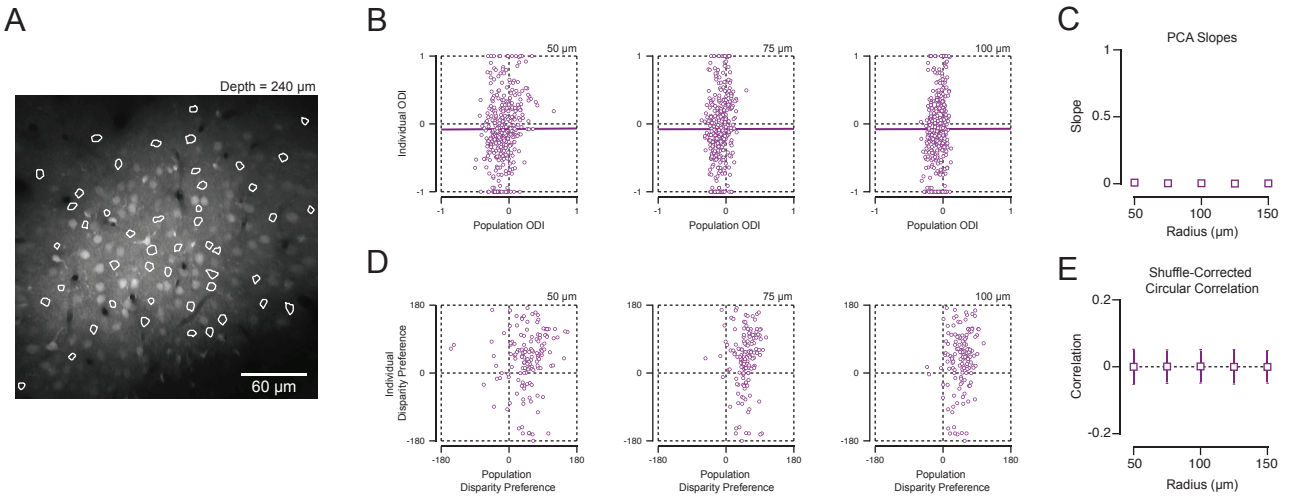


**Supplementary Figure 5: Patches of neuropil activity lack functional relationship with population aggregates (see Figure 4)**

(A) Two-photon image of OGB-1 at single focal plane (depth = 240 µm). Individual ROIs collecting patches of neuropil activity are shown (white outlines). ROIs were drawn to exclude in-focus fluorescence from neurons and astrocytes. (B) Plots of ocular dominance for individual neuropil patches and local population averages, for different radii (50-100 µm). Lines are major axis slope from Bootstrapped PCA (see Methods). All data presented are from a single animal. (C) Spatial dependence of relationship between individual neuropil patch and local population average ocular dominance. Shown is mean Bootstrapped PCA slope and standard error across radii. (D) Disparity preference for individual neuropil patches and local population averages, across different radii (50-100 µm). Data include only tuned neuropil patches (DSI > 0.1). Clustering of population preference represents bias in sample population, evident because the data presented are from a single animal. (E) Spatial dependence of relationship between individual neuropil patch and local population average disparity preference. Shown are shuffled-corrected mean circular-correlation and standard error across radii.

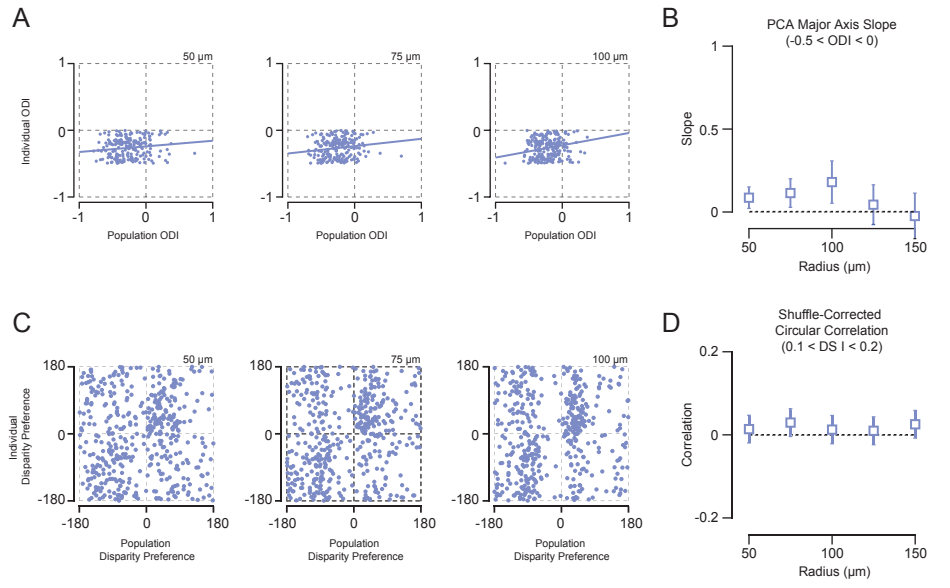


**Supplementary Figure 6: No spatial relationship for PV- neurons with similar binocular response properties as PV+ interneurons (see Figure 4)**

(A) Plots of individual PV- interneuron ocular dominance and local population vector average, for different radii (50-100 µm). These data include only PV- neurons with similar eye preference as PV+ interneurons (-0.5 < ODI < 0). (B) Spatial dependence of relationship between individual cell and local population averages. Shown is mean Bootstrapped PCA slope and standard error across radii. (C) Plots of individual PV- neuron disparity preference and local population vector average, for different radii (50-100 µm). These data include only PV- neurons moderately selectivity for disparity (0.1 < DSI < 0.2). (D) Spatial dependence of relationship between individual cell and local population averages. Shown are shuffled-corrected circular-correlations across radii.